A Single-Cell Transcriptome Atlas of the Adult Human Retina

Samuel W. Lukowski[1,#], Camden Y. Lo[2,#], Alexei Sharov[3], Quan Nguyen[1], Lyujie Fang[4,5,6], Sandy S.C. Hung[4,5], Ling Zhu[7], Ting Zhang[7], Ulrike Grünert[7], Tu Nguyen[4,5], Anne Senabouth[1,15], Jafar S. Jabbari[8], Emily Welby[9], Jane C. Sowden[9], Hayley S. Waugh[10], Adrienne Mackey[10], Graeme Pollock[10], Trevor D. Lamb[11], Peng-Yuan Wang[12,13], Alex W. Hewitt[4,5,14], Mark Gillies[7], Joseph E. Powell[1,15,^], Raymond C.B. Wong[4,5,16,^]

[1] Institute for Molecular Bioscience, University of Queensland, Australia
[2] Monash University, Australia
[3] National Institute for Aging, National Institutes of Health, United States
[4] Centre for Eye Research Australia, Australia
[5] Ophthalmology, Department of Surgery, University of Melbourne, Australia
[6] Jinan University, China
[7] Save Sight Institute, University of Sydney, Australia
[8] Australian Genome Research Facility, Australia
[9] Stem Cells and Regenerative Medicine Section, NIHR Great Ormond Street Hospital Biomedical Research Centre, UCL Great Ormond Street Institute of Child Health, UK
[10] Lions Eye Donation Services, Australia
[11] John Curtin School of Medical Research, The Australian National University, Australia
[12] Department of Chemistry and Biotechnology, Swinburne University of Technology, Australia
[13] Center for Human Tissues and Organs Degeneration, Institute of Biomedicine and Biotechnology, Shenzhen Institute of Advanced Technology, Chinese Academy of Science, China
[14] Menzies Institute for Medical Research, University of Tasmania, Australia
[15] Garvan-Weizmann Centre for Cellular Genomics, Garvan Institute of Medical Research, Australia
[16] Shenzhen Eye Hospital, China

This is the author manuscript accepted for publication and has undergone full peer review but has not been through the copyediting, typesetting, pagination and proofreading process, which may lead to differences between this version and the Version of Record. Please cite this article as doi: 10.15252/EMBJ.2018100811

equal first-authors.
^ equal senior-authors

Lead contact/correspondence: Dr Raymond Wong, Centre for Eye Research Australia, Level 6, 75 Commercial Road, Melbourne, VIC 3004, Australia; Phone: +613 85321962; email: wongcb@unimelb.edu.au

Summary

The retina is a specialized neural tissue that senses light and initiates image processing. Although the functional organisation of specific retina cells have been well-studied, the molecular profile of many cell types remains unclear in humans. To comprehensively profile the human retina, we performed single cell RNA-sequencing on 20,009 cells from three donors and compiled a reference transcriptome atlas. Using unsupervised clustering analysis, we identified 18 transcriptionally distinct cell populations representing all known neural retinal cells: rod photoreceptors, cone photoreceptors, Müller glia, bipolar cells, amacrine cells, retinal ganglion cells, horizontal cells, astrocytes and microglia. Our data captured molecular profiles for healthy and putative early degenerating rod photoreceptors, and revealed the loss of *MALAT1* expression with longer post-mortem time, which potentially suggested a novel role of *MALAT1* in rod photoreceptor degeneration. We have demonstrated the use of this retina transcriptome atlas to benchmark pluripotent stem cell-derived cone photoreceptors and an adult Müller glia cell line. This work provides an important reference with unprecedented insights into the transcriptional landscape of human retinal cells, which is fundamental to understanding retinal biology and disease.

Keywords

Retina, transcriptome, single cell RNA sequencing, photoreceptor subtypes

Introduction

The eye is a highly specialised sensory organ in the human body. Sight is initiated by the conversion of light into an electrical signal in the photoreceptors of the neurosensory retina. The rod photoreceptors are responsible for light detection at extremely low luminance, while the cone photoreceptors are responsible for colour detection and operate at moderate and higher levels. Following preprocessing, by horizontal, bipolar and amacrine cells, the resultant signal is transferred via ganglion cells to the brain. Neurotransmitter support is provided by Müller glia, retinal astrocytes and microglial cells. Inherited retinal diseases are becoming the leading cause of blindness in working age adults, with loci in over 200 genes associated with retinal diseases (RetNet: https://sph.uth.edu/retnet/), often involving specific retinal cell types. Knowledge of the transcriptome profile of individual retinal cell types in humans is important to understand the cellular diversity in the retina, as well as the study of retinal genes that contribute to disease in individual retinal cell types. (Hornan *et al*, 2007a; Mustafi *et al*, 2016a; Whitmore *et al*, 2014a; Farkas *et al*, 2013a; Pinelli *et al*, 2016a)

The transcriptome profiles of whole human retina from adults (Hornan *et al*, 2007b; Mustafi *et al*, 2016b; Whitmore *et al*, 2014b; Farkas *et al*, 2013b; Pinelli *et al*, 2016b) and during fetal development (Hoshino *et al*, 2017; Kozulin *et al*, 2009) have been previously described. However, these studies only assayed the averaged transcriptional signatures across all cell types, meaning that information on the cellular heterogeneity in the retina is lost. As such, the transcriptional pathways that underlie the highly specialised function of many human retinal cell types remain unclear; including the rod and cone photoreceptors, Müller glia cells, horizontal cells, and amacrine cells. Recent advances in RNA sequencing and microfluidic platforms have dramatically improved the accessibility of single cell transcriptomics, with increased throughput at a lower cost. Critically, single-cell microfluidics and low-abundance RNA library chemistries allow accurate profiling of the transcriptome of individual cell types. This has been demonstrated in the mouse, where transcriptome profiles of the mouse retina (Macosko *et al*, 2015) and retinal bipolar cells (Shekhar *et al*, 2016) have been described at the single cell level using the Drop-seq method (Macosko *et al*, 2015). These studies provided a molecular classification of the mouse retina and identified novel markers for specific cell types, as well as novel candidate cell types in the retina. Recently, single cell transcriptomics was used to analyse the human retina. Phillips et al. have profiled a total of 139 cells from adult retina using the C1 Fluidigm platform (Phillips *et al*, 2018), but the limited number of profiled cells presents challenges in the annotation and accurate identification of individual retinal cell types. Moreover, a flow cytometry approach was used to isolate 65 human fetal cone photoreceptors followed by scRNA-seq profiling (Welby *et al*, 2017). During the preparation of this manuscript, Voigt et al. reported scRNA-seq profiling of 8,217 cells from human retina obtained from a mixed pool of donors that included a healthy patient, a patient with early glaucoma and one with unknown ocular history (Voigt et al. 2019),

Herein we report the generation of a human neural retina transcriptome atlas using 20,009 single cells collected from three healthy donors. Our data provide new insights into the transcriptome profile of major human retinal cell types and establish a high cellular-resolution reference of the human neural retina, which will have implications for identification of biomarkers and understanding retinal cell biology and diseases.

Results

Preparation of human neural retinal samples and generation of single cell transcriptome atlas

We obtained post-mortem human adult eyes approved for research purposes following corneal transplantation. As the transcriptome profile of human retina pigment epithelium cells has already been reported (Strunnikova *et al*, 2010; Liao *et al*, 2010), we focused solely on the neural retina layers. In this study we extracted the neural retina from twelve donor eyes (Appendix Table S1). We observed consistent cell viability across retinal tissues retrieved within 15 hours post-mortem (Appendix figure S1A) and found that donor age does not impact negatively on cell viability in the extracted neural retina (Appendix figure S1B). To minimize potential risk of mRNA degradation due to reduced cell viability, we selected three donor samples retrieved within 15 hours post-mortem and analysed them with single cell RNA sequencing (scRNA-seq) using the 10X Genomics Chromium platform.

Sequence data from five scRNA-seq libraries derived from the three neural retinal samples were pooled for processing and analysis. From 23,000 cells, we obtained an average of 40,232 reads per cell and 1,665 UMIs (unique transcripts) per cell. Following quality control and filtering using the Seurat package (Butler *et al*, 2018), our final dataset contained 20,009 cells, which were taken forward for further analysis.

The scRNA-seq data was initially analysed using an unsupervised graph clustering approach implemented in Seurat (version 2.2.1) to classify individual cells into cell populations according to similarities in their transcriptome profiles. Overall, the cells were classified into 18 transcriptionally distinct clusters (Appendix figure S2). We first assessed the variation between donor samples (Appendix table S2). Interestingly, although many of the identified clusters are well represented in all three donor retinal samples, we also observed several donor-specific clusters corresponding to rod photoreceptors (Appendix figure S3A). In contrast, we observed minimal variation between two different libraries prepared from the same donor sample, supporting the quality of the scRNA-seq datasets in this study (Appendix figure S3B). The average expression for all detected genes in each cluster are listed in Dataset EV1.

Identification of major cell types in the human retina using scRNA-seq

Based on known markers (Klimova *et al*, 2015; Vecino *et al*, 2016; Shekhar *et al*, 2016; Macosko *et al*, 2015; Soto *et al*, 2008; Imanishi *et al*, 2002; Blackshaw *et al*, 2001; Corbo *et al*, 2007), we were able to assign cell identities to the 16 of the 18 clusters (Figure 1A-1D), corresponding to rod photoreceptors (*PDE6A, CNGA1, RHO*), cone photoreceptors (*ARR3, GNGT2, GUCA1C*), Müller glia (*RLBP1/CRALBP*), retinal astrocytes (*GFAP*), microglia (*HLA-DPA1, HLA-DPB1, HLA-DRA*), bipolar cells (*VSX2, OTX2*), retinal ganglion cells (*NEFL, GAP43, SNCG*), amacrine cells (*GAD1, CALB1, CHAT*) and horizontal cells (*ONECUT1, ONECUT2*). The expression of selected marker genes are displayed in *t*-SNE plots (Figure 1D). Two clusters (C5 and C14) express markers from multiple retinal cell types (Appendix figure S4), thus we were unable to assign cell identities to these 2 clusters and they were excluded from further analysis. Interestingly, our data demonstrated multiple transcriptionally distinct clusters within the rod photoreceptors (6 clusters) and bipolar cells (3 clusters). In contrast, only one cluster was detected for cone photoreceptors, Müller glia, retinal ganglion cells, horizontal cells, amacrine cells, retinal astrocytes and microglia respectively. Correlation analysis confirmed the similarity between clusters within the same cell type (Figure 1E). As expected, we observed high correlations between the expression levels of transcripts within photoreceptor cell types (rod and cones), as well as glial cells (retinal astrocytes and Müller glia) and other retinal neurons (bipolar cells, retinal ganglion cells, amacrine cells and horizontal cells). The composition of cell populations across our three donors show that the majority of the cells in human neural retina were rod photoreceptors (~74%) followed by bipolar cells (~10%) . These results are similar to those reported in mice, where rod photoreceptors and bipolar cells form the majority of cells in the retina (Jeon *et al*, 1998; Macosko *et al*, 2015).

To identify genes whose expression was specific to a given cell type, we performed differential gene expression analysis to identify marker genes for each cluster (Figure 1F). We subsequently extracted membrane-related proteins from gene ontology annotations to identify potential surface markers, which can be used to develop immuno-based methods to isolate primary culture of individual retinal cell types. Appendix table S3 lists the identified markers for individual retinal cell types. We also assessed the gene expression of a panel of commonly known markers in amacrine cells and bipolar cells (Figure EV1-2), as well as a panel of markers for subtype identification recently identified in mouse scRNA-seq studies (Shekhar *et al*, 2016; Macosko *et al*, 2015). In particular, the bipolar clusters can be classified as OFF-bipolar cells (*GRIK1*+: C6) and ON-bipolar cells (*ISL1*+: C8, C11). Further analysis showed that C8 represents rod bipolar cells based on the marker *PRKCA*, while C11 expresses the marker *TTR* corresponding to a diffuse bipolar subtype DB4 (Figure EV1). In summary, we profiled the transcriptomes of all major cell types in the human retina in the presented dataset. Due to their abundance, for the subsequent analyses we focused on the photoreceptors and glial cells.

Profiling healthy and degenerating human rod photoreceptor subpopulations

We profiled 14,759 rod photoreceptors and showed that they can be classified into six populations with distinct gene expressions (c0, c1, c2, c3, c4, c7). We assessed these six clusters with a panel of seven known rod or pan-photoreceptor markers (Figure 2A). Our results suggest differential expression patterns among the seven markers. All seven rod markers are highly abundant, consistent with previous scRNA-seq studies of mouse and human retina (Phillips *et al*, 2018; Macosko *et al*, 2015). The seven markers showed differential expression patterns in the six identified rod photoreceptor clusters. In particular, *RHO, GNGT1* and *SAG* have the highest levels of rod marker detected, followed by *NRL*, *ROM1*, *GNAT1* and *CNGA1*. We also noted that *ROM1* is expressed in both rod and cone photoreceptors, which is consistent with previous studies (Boon *et al*, 2008). Importantly, many rod photoreceptor clusters consist of a majority of cells from a single donor (>90% for c0, c2, c4 and >80% for c1, c7; Figure 2B). It is possible that this observation is due to the systematic biases such as differences in tissue retrieval time, age of donors, or other sample preparation variation. The exception is cluster c3, which is well represented by all three donors.

Next we set out to further define and classify heterogeneity in rod photoreceptors. We observed that *MALAT1*, a long non-coding RNA that plays a role in retinal homeostasis and disease (Wan *et al*, 2017), was robustly expressed in ~66% of the identified rod photoreceptors (9,750 cells) while the rest had little to no expression (5,009 cells; Figure 2C). As such, we utilized *MALAT1* expression as a discriminator and investigated differences between rod photoreceptors with high expression (*MALAT1-hi*; > 4.68 normalised transcripts per cell) or low expression (*MALAT1-lo*; < 4.68 normalised transcripts per cell). *MALAT1-hi* and *-lo* rod photoreceptors were consistently found in each donor and library samples, with *MALAT1-hi* accounting for ~66%, 90% and 36% of the rods in donors #1, #2 and #3 respectively (Figure 2D). To further validate this finding, we performed RNA *in situ* hybridization in another three donor retinal samples. We consistently observed the presence of *MALAT1-hi* and *-lo* subpopulations of rod photoreceptors in all retinal samples (Figure 2E, Figure EV3A). Together, these results showed the presence of heterogeneity within rod photoreceptors that can be distinguished by *MALAT1* expression.

To rule out the possibility that the presence of *MALAT1* rod subpopulations is due to donor sample variations, we applied Canonical Correlation Analysis (CCA) to correct for technical and batch artefacts. We found that CCA can effectively corrected the donor-specific effect on rod photoreceptor clusters (Figure 3A and 3B). The average expression for all detected genes in each cluster are listed in Dataset EV2. Following CCA correction, we identified three rod photoreceptors clusters (CCA0, CCA1, CCA10), which expressed a panel of seven rod photoreceptor markers and were well represented in all donor samples (Figure 3C). Notably, the majority of cells in CCA0 were low in *MALAT1* expression, while CCA1 and CCA10 represented *MALAT1-hi* rod subpopulations (Figure 3D and 3E). This is consistent with our RNA *in situ* hybridization analysis, where we consistently observed *MALAT1-hi* and *-lo* subpopulations of rod photoreceptors in all retinal samples (Figure EV3A). Collectively these results provide evidence that *MALAT1* heterogeneity in rod photoreceptors is not due to inter-individual variability.

We also considered the possibility that *MALAT1-lo* rod subpopulations may represent an artefact of 'low quality cells' in scRNA-seq data, due to a low number of sequencing reads or broken cell membrane. In this regard, up-regulated levels of mitochondrial-encoded genes and ribosomal proteins can be used to identify such low quality cells in scRNA-seq data (Ilicic *et al*, 2016). For our scRNA-seq dataset, we did not observe upregulation in gene expression for a panel of ribosomal proteins (*RPL41, RPLP1, RPL21, RPS27, RPL13A, RPL36, RPL39* and *RPS28*; Figure 3F). However, the rod cluster CCA10, representing 1.4% of rod photoreceptor cells, showed markedly increased levels of mitochondrial-encoded genes (*MT-CO2, MT-ND5, MT-ND3, MT-CYB, MT-ND1, MT-ND2, MT-CO3, MT-ATP6, MT-CO1, MT-ND4*; Figure 3G*)*, suggesting that CCA10 represented a low-quality *MALAT1-hi* rod cluster and was excluded from further analysis.

As we utilised post-mortem retinal samples in this study, we reasoned that *MALAT1-lo* subpopulation may potentially reflect the early stages of post-mortem degeneration in rod photoreceptors. To determine this, we extracted retinal samples from the same donor at different time points of progressive post-mortem degeneration, with longer time points predicted to have more stressed/dying photoreceptors. Our results showed that there was a high proportion of *MALAT1-hi* rod photoreceptors at 7 hours post-mortem (Figure 4, ~95%). However, we observed a marked decrease in *MALAT1* expression in rod photoreceptors at 13 hours post-mortem. Similar results were observed for the three retinal samples processed for scRNA-seq (Figure EV3B). Together, these results demonstrated that *MALAT1* is a novel marker for healthy photoreceptors with loss of expression potentially preceding putative cell degeneration. In summary, we showed that scRNA-seq can be used to profile healthy (CCA1) and degenerating rod photoreceptors (CCA0), which can be distinguished by high or low *MALAT1* expression levels respectively.

Transcriptome profile of cone subtypes in the human retina

We detected 564 cone photoreceptor cells in our scRNA-seq data, which are distinguishable from the other cell types by the expression of the cone marker genes *ARR3, CNBG3, GNAT2, GNGT2, GRK7, GUCA1C, PDE6C, PDE6H, OPN1LW, RXRG* and *THRB* (Figure 5A). All 11 marker genes analysed show specific expression patterns in the cone cluster (C10). We set out to further assess the composition of the cone cluster. In humans, there are three identified subtypes of cone photoreceptor which can be distinguished by expression of a sole opsin gene: *OPN1SW*-positive S-cones, *OPN1MW*-positive M-cones and *OPN1LW*-positive L-cones respond preferentially to shorter, medium and longer wavelengths responsible for colour vision (Roorda & Williams, 1999). Notably *OPN1LW* and *OPN1MW* exhibit ~98% sequence homology and are unable to be distinguished by 3' sequencing utilised in this study. By quantifying the number of cells that express the opsin genes, our results showed that the majority of the cone cluster are L/M cones (73.22%) and S-cones in much lower proportion (3.19%, Figure 5B), at levels consistent with those estimated by a previous adaptive optics and photo-bleaching study (Roorda & Williams, 1999). As expected, the identified cone photoreceptors only express either *OPN1SW* or *OPN1LW/MW* (Figure 3C).

To further study the molecular differences and identify molecular markers for the cone subtypes, we performed differential gene expression analysis to determine genes that can distinguish the cone subtypes. Our results identified a panel of genes that differentially marked S-cones (e.g. *CCDC136*, *RAMP1*, *LY75, CADM3, TFPI2, CRHBP, RAB17, UPB1, RRAD, SLC12A1*) and L/M-cones (e.g. *THRB, KIF2A, LBH, PGP, CHRNA3, AHI1, LIMA1*; Figure 3D). We compared this list of cone subtype genes to those identified in scRNA-seq studies of the macaque and mouse retina, and showed that a number of the cone subtype genes in human are conserved in macaque and mouse (Macosko et al. 2015; Peng et al. 2019), including S-cone marker *CCDC136* and L/M-cone marker *THRB*. Interestingly, *CCDC136* is located next to the *OPN1SW* locus in human and could possibly be co-regulated at the transcriptional level. The thyroid hormone receptor *THRB* is required for the development of M-cones in mice (Ng *et al*, 2001) and L/M cones in humans as determined by pluripotent stem cell model (Eldred *et al*, 2018). Notably, there are two known receptor isoforms for THRB (TRβ1 and TRβ2) and further research to determine the precise roles of THRB isoforms in subtype specification of human cones would be of great interest. Moreover, the transcription factor *TBX2* has been implicated in subtype specification of *Sws1*-cones in zebrafish and chicken (Alvarez-Delfin *et al*, 2009; Enright *et al*, 2015). In support of these studies, our data showed that *TBX2* marks the S-cones in human which is also conserved in macaque (Peng *et al*, 2019). Together these results detailed the molecular profiles and identified marker genes that can distinguish the cone subtypes in human.

Assessment of glial cells in human retina

Next, we focused on two related glial cell types in the human retina, the Müller glia and the retinal astrocytes. Our scRNA-seq data has profiled a total of 2,723 Müller glia cells which classified into a single cluster (C9) and 49 retinal astrocytes which form a single cluster (C16). Figure 5E shows the expression of a panel of 9 commonly used markers for Müller glia and retinal astrocytes. Our results demonstrated that many of these markers are present in both Müller glia and retinal astrocytes at differential expression levels. *VIM, GLUL* and *S100A1* marked both Müller glia and retinal astrocytes at high expression levels. *GFAP* represents a reliable marker for retinal astrocytes, and its expression is consistent with a previous report (Vecino *et al*, 2016). Notably, Müller glia are low in *GFAP* expression, indicating they are not in an activated state commonly caused by stresses and reactive gliosis (Fernández-Sánchez *et al*, 2015). The *S100B* is also expressed in retinal astrocytes at varying levels but absent in Müller glia. Conversely, Müller glia can be distinguished from retinal astrocytes by high expression levels of *RLBP1*, and *RGR* to a lesser extent. Together these results provide insights into the differential expression patterns of known glial markers in Müller glia and retinal astrocytes in human.

As glial cell proliferation has been linked to a range of pathological conditions including retinal gliosis and retinal injury (Subirada *et al*, 2018), this provides a means of assessing the health of the profiled retinas. We assigned a cell cycle phase score to each cell using gene expression signatures for the G1, S, G2, and G2/M phases (Kowalczyk *et al*, 2015); Figure EV4). We determined that most of the Müller glial cells expressed genes indicative of cells in G1 phase (75%), suggesting they are not proliferative. These results demonstrated the absence of hallmarks of gliosis/retinal injury and support the quality of the donor retinas profiled.

Using the human neural retina transcriptome atlas for benchmarking

To demonstrate the use of our dataset as a benchmarking reference, we compared the scRNA-seq profiles of distinct cell types generated using alternative methods, including fetal human cone photoreceptors, human induced pluripotent stem cell derived-cone photoreceptors (hiPSC-cone; (Welby *et al*, 2017), and a sample of adult human retina with 139 cells (Phillips *et al*, 2018). Correlation analysis demonstrated that the adult human retina sample showed highest similarity to rod photoreceptor (0.63, Figure EV5), which is expected as rod photoreceptors represent the majority of the cells in the retina. Interestingly, our results also showed that the transcriptome of hiPSC-cone after 15 weeks of differentiation exhibited the highest similarity to cone photoreceptors, and low similarities to all other retinal cell types (Figure 6A, EV5). In particular, hiPSC-cone showed high similarities to fetal cone photoreceptors and adult cone photoreceptors (0.71 and 0.61 respectively), and a much lower similarity to adult rod photoreceptors (0.33). In support of this, principal component analysis demonstrated that the hiPSC-cone are closer to fetal cone photoreceptors, rather than the adult counterpart (Figure 6B). These results confirmed direct differentiation of hiPSCs to cone photoreceptors with good quality, and the hiPSC-derived cone photoreceptors are closer to fetal origin compared to their adult counterpart.

In another benchmarking example, we set out to assess the potential differences between *in vitro* cell lines compared to adult cells *in vivo*. In this regard, we compared the spontaneously immortalised human Müller glia cell line MIO-M1 (Lawrence *et al*, 2007; Limb *et al*, 2002) to all the retinal cell types identified in our dataset. Using scRNA-seq, we profiled 7,150 MIO-M1 cells with 23,987 reads per cell post-normalization corresponding to 3,421 detected genes. Unsupervised clustering and t-SNE analysis showed that the MIO-M1 cells formed one cluster that is transcriptionally distinct from all retina cell types identified in the human neural retina dataset (Fig 6C). Correlation analysis showed that MIO-M1 displayed similarities to retinal glial cells, with higher similarity to astrocytes compared to Müller glia (0.63 and 0.46 respectively, Fig 6D). In particular, we identified that MIO-M1 express high levels of thymosin beta 4 gene (*TMSB4X*), which has been linked to glioma malignancy (Wirsching *et al*, 2013), as well as the calcyclin gene (*S100A6*), which is implicated in macular or cone associated diseases (Yoshida *et al*, 2004; Figure 5E). Together, our results highlighted the similarities and differences of MIO-M1 to adult retinal glial cells in human.

Discussion

The data presented here describe the generation of a detailed reference transcriptome atlas of the human neural retina at the single-cell level. The establishment of reference transcriptome maps for individual cell types in the retina provide unprecedented insights into the signals that define retinal cell identity and advance our understanding of the retina. This human neural retina transcriptome data can be used as a benchmark to assess the quality and maturity of pluripotent stem cell-derived retinal cells, such as retinal ganglion cells (Gill *et al*, 2016; Kobayashi *et al*, 2018; Sluch *et al*, 2015) and photoreceptors (Lakowski *et al*, 2018). We obtained a mean sequencing depth of 40,232 reads per cell across 23,000 cells, which enabled us to confidently classify the majority of cell types in a complex tissue like the retina. We confirmed that this sequencing depth is sufficient to identify the major cell types. For less transcriptionally distinct cell types, including amacrine and retinal ganglion cells, the ability to resolve subtypes might be improved by increased sample size, greater cell numbers or ultra-deep sequencing of those populations. Also, regarding post-mortem time for the donor retina, we found that at the transcriptome levels there are no obvious variations in all major cell types in neural retina retrieved from 6-14 hours postmortem, with the exception of rod photoreceptors. This potentially suggested that the rod photoreceptors are more sensitive to putative post-mortem degeneration compared to other retinal cell types. Further studies to optimise methods to preserve donor retinal tissues will help to minimize post-mortem effects prior to scRNA-seq processing.

One of the most interesting observations is the presence of heterogeneous subpopulations within known retinal cell types. This highlights the sensitivity of using a scRNA-seq approach to capture and classify retinal cell types in an unbiased manner. In particular, our results demonstrated the presence of two rod photoreceptor subpopulations in post-mortem retina that display differential expression of *MALAT1*. Notably, the presence of *MALAT1-hi* and *-lo* rod subpopulations were consistently observed in all post-mortem samples analysed (n=7). We further showed that *MALAT1-lo* subpopulations represent putative early degenerating rod photoreceptors, a finding that has not previously been reported in human or any other species. We also noted that there is some heterogenous *MALAT1* expression in other retinal cell types in human, albeit to a lesser extent compared to rod photoreceptors. Previous studies have demonstrated a role of *MALAT1* in regulating the survival of retinal ganglion cells (Li *et al*, 2017) and in pathogenesis of retinal pigment epithelium cells (Yang *et al*, 2016). However, the functional role of *MALAT1* in photoreceptors remained unclear. Our results demonstrated the loss of *MALAT1* expression in rod photoreceptors following longer post-mortem time with putative degeneration, and suggests *MALAT1* as a potential target to enhance rod photoreceptor survival and retinal preservation. Future studies are warranted to investigate the functional role of *MALAT1* in photoreceptors, as well as other retinal cell types in human. Our transcriptome data also revealed rod photoreceptor clusters specific to particular donor retinas and we showed that application of the CCA method could effectively correct for these donor/batch variations in rod photoreceptors. Further studies with a larger number of donor samples will allow testing of the feasibility of using scRNA-seq to comprehensively analyse the retina in different individuals, such as assessment of the effects of aging or degenerative retinal diseases.

Another outcome of this study is the assessment of biomarkers that allow identification of major retinal cell types and subtypes. Our results provide new insights into the cone photoreceptor subtypes in human. The cone subtypes are traditionally categorized based on expression of different opsins that allowed for cellular detection of light at various wavelengths. While the S-cones are structurally different from the other two cone subtypes, the L-cones and M-cones are structurally similar and difficult to distinguish from each other, except for the opsin they expressed (Viets *et al*, 2016). We report the first description of the transcriptome profiles of S-cones in adult human and highlight novel marker genes that can be used to distinguish them. We also identified the transcriptome and novel marker genes for L/M-cones, however given the high sequence homology, particularly at the 3' end, of *OPN1MW* and *OPN1LW*, we could not confidently separate L-cones and M-cones. In addition, we show that many of the known Müller glia markers are often expressed in retinal astrocytes, and we also provide a detailed assessment of commonly used retinal glial markers showing the differential expression pattern between Müller glia and retinal astrocytes. Furthermore, we determined that multiple genetic markers, based on binary and/or gradient expression profiles, were required to improve the classification of clustered cell populations. More detailed classification of highly similar cell types may be possible through the combination of single cell mRNA and protein measurements using barcoded antibodies, as implemented in the CITE-seq method (Stoeckius *et al*, 2017).

Finally, our results highlighted the use of this neural retina transcriptome atlas to benchmark retinal cells derived from stem cells or primary cultures. A major goal of pluripotent stem cell research is to derive cells that are similar to those in adults *in vivo*, which is important for development of stem cell disease models and regenerative medicine (Hung *et al*, 2017). Our analysis shows that hiPSC-derived cone photoreceptors are highly similar to both fetal and adult cones in comparison with all other major retinal cell types. We show that hiPSC-derived cells are more fetal-like than adult-like, which is consistent with other studies (Handel *et al*, 2016; Baxter *et al*, 2015). We also benchmark a commonly used Müller glia cell line MIO-M1 (Lawrence *et al*, 2007; Limb *et al*, 2002). Our results showed that while this cell line exhibits similarities to adult retinal glial cells, there are also some differences between MIO-M1 and adult Müller glia, such as high expression of the glioma-related gene thymosin beta 4 (*TMSB4X)* in MIO-M1. Previous reports have also described differences in gene expression in MIO-M1 to Müller glia, and showed that MIO-M1 express markers for post-mitotic retinal neurons and neural stem cells (Lawrence *et al*, 2007; Hollborn *et al*, 2011). Our results and others highlighted the potential effects of prolonged *in vitro* culture of primary retinal cells. Collectively, we showed that the human neural retina transcriptome atlas provides an important benchmarking resource to assess the quality of derived retinal cells, which would have implications for stem cell and neuroscience research.

One of the limitations of this study is the finite number of profiled cell types less frequently represented in the retina such as the amacrine cells and the retinal ganglion cells, which are known to be highly complex. The presented dataset is limited in power to accurately identify differences in the transcriptomes of the subtypes in amacrine and retinal ganglion cells. With the identification of surface markers for these retinal cell types in this study, this work lays the foundation for future research using selection and enrichment (Shekhar *et al*, 2016) of these and other retinal cell types to improve the resolution of the human neural retina transcriptome atlas. Two recent studies have reported the use of surface marker to preselect or enrich for microglia (Masuda *et al*, 2019) and bipolar cells (Peng *et al*, 2019) in human tissues prior to scRNA-seq, which provided a feasible strategy to increase sensitivity to profile cell types less frequently represented. Another limitation is the use of 3' gene expression profiling, which presents a challenge for distinguishing L-cones and M-cones. Given the high sequence homology of *OPN1LW* and *OPN1MW* (98%), future studies using full-length mRNA sequencing of single cone photoreceptor cells would provide greater distinction and classification accuracy of the *OPN1MW* and *OPN1LW*-positive cells. Future studies to increase the donor sample size, number of profiled cells with improved capture technologies will further improve the resolution of this human retina transcriptome atlas, allowing more accurate cell type classification and greater statistical power to determine molecular differences between cell populations.

This study describes the transcriptome of human neural retina at a single cell level which identified the transcriptome of all major human retinal cell types. Our findings shed light on the molecular differences between subpopulations within the rod photoreceptors and the cone photoreceptors. The presented dataset provides an important roadmap to define the genetic signals in major cell types in the human retina and can be used as a benchmark to assess the quality of stem cell-derived cells or primary retinal cells.

Online Methods

Human retina collection

Collection of donor samples was approved by the Human Research Ethics committee of the Royal Victorian Eye and Ear Hospital (HREC13/1151H) and Save Sight Institute (16/282) and carried out in accordance with the approved guidelines. Informed consent was obtained from all donors and that the experiments conformed to the principles set out in the WMA Declaration of Helsinki and the Department of Health and Human Services Belmont Report. For scRNA-seq, post-mortem eye globes were collected by the Lions Eye Donation Service (Royal Victorian Eye and Ear Hospital) for donor cornea transplantation. The remaining eye globes were used for dissection to extract the neural retina. The lens, iris and vitreous were removed and the choroid/RPE layers were excluded from the sample collection. Following extraction, the neural retinal samples were dissociated and processed for scRNA-seq right away. Neural retina samples were dissociated into single cells in dissociation solution (2mg/ml papain, 120 Units/ml DNase I) for 15 minutes. The dissociated neural retina was filtered to ensure single cell suspension using a 30µm MACS Smart Strainer (Miltenyi). For sample from Patient SC, the Dead Cell Removal kit (Miltenyi) was utilised to remove dead cells prior to scRNA-seq. However, in our hands we found that the Dead Cell Removal kit only had a modest improvement in the cell viability (~8% improvement, data not shown).

Single cell RNA sequencing (scRNA-seq)

Single cells from three independent neural retina samples were captured in five batches using the 10X Chromium system (10X Genomics). The cells were partitioned into gel bead‑in‑emulsions and barcoded cDNA libraries, then prepared using the single cell 3' mRNA kit (V2; 10X Genomics). Single cell libraries were sequenced in 100bp paired-end configuration using an Illumina Hi-Seq 2500 at the Australian Genome Research Facility.

Bioinformatics processing

The 10X Genomics *cellranger* pipeline (version 2.1.0; (Zheng *et al*, 2017) was used to generate fastq files from raw Illumina BCL files (*mkfastq*). To generate read count matrices from the fastq files, we used *cellranger count*, which uses the STAR aligner (Dobin *et al*, 2013), to map high quality reads to the transcriptome (GRCh38) and performs UMI counting. To overcome the stringent threshold implemented in *cellranger* that discards real cells under certain conditions, such as populations of cells with a low RNA content, the --*force-cells* parameter was set to 3000 for the donor 1 library and 5000 for donor 2 and 3 libraries. Using the barcode rank plots produced by cellranger, these parameters were selected to increase the number of detected cells for further analysis. The *cellranger* aggregation function (*aggr*) was used to combine the 5 libraries and normalize the between-sample library size differences.

Count data was imported into the Seurat single cell analysis software (v2.0.1; https://github.com/satijalab/seurat) and quality control of sequenced libraries was performed to remove outlier cells and genes. Cells with 200-2500 detected genes and expressing < 10% mitochondrial genes were retained. Genes were retained in the data if they were expressed in ≥ 3 cells. Additional cell-cell normalization was performed using the LogNormalize method, and inherent variation caused by mitochondrial gene expression and the number of unique molecular identifiers (UMIs) per cell was regressed out.

Clustering at a resolution of 0.6 was performed on PCA-reduced expression data for the top 20 principal components using the graph-based shared nearest neighbour method (SNN) which calculates the neighborhood overlap (Jaccard index) between every cell and its nearest neighbors. Clustering results were visualised using t-distributed stochastic neighbour embedding (t-SNE). Individual samples and sample groups were also visualised using t-SNE.

Prediction of the cell cycle phase of individual retinal cells was performed in Seurat using cell cycle-specific expression data (Kowalczyk *et al*, 2015). Briefly, genetic markers associated with G2/M and S phase were used to assign cell scores, and cells expressing neither of the G2/M or S phase markers were classified as being in G1 phase.

Sequencing data for fetal (scRNA-seq) and hiPSC-derived cone photoreceptors (bulk RNA-seq) was obtained from ArrayExpress using the accession numbers E-MTAB-6057 and E-MTAB-6058 (Welby *et al*, 2017). Gene expression matrices were generated from the fastq files using the STAR aligner software. scRNA-seq data from 72 cells were quality-controlled, filtered and then normalised with the scran algorithm (Lun *et al*, 2016) as described (Welby *et al*, 2017), using the *ascend* (https://github.com/IMB-Computational-Genomics-Lab/ascend) package in R, which resulted in 63 high quality single cell transcriptomes. Bulk RNA-seq data generated from 6 hiPSC-derived cone photoreceptor cultures was filtered such that each gene was represented by at least 10 counts in all samples and normalisation was performed in edgeR using the trimmed mean of M method (Robinson & Oshlack, 2010). Pre-processed scRNA-seq data generated from adult retina (Phillips *et al*, 2018) was obtained from the Gene Expression Omnibus (GSE98556).

Canonical correlation analysis

Canonical correlation analysis (CCA) was applied to correct donor-specific effects observed in the rod photoreceptor populations. This was achieved by separating the raw data into 5 sample-specific datasets, which were then used as inputs for the RunMultiCCA function in Seurat. For the CCA analysis, we used the most highly variable genes that were shared by all 5 samples and the recombined data was aligned using the first 20 CC dimensions, selected by biweight midcorrelation (bicor) analysis. Aligned cells were reclustered in Seurat using the first 20 aligned CC dimensions at a resolution of 0.6.

Identification of retinal cell types

Cell types were classified using differential expression analysis, which compared each cluster to all others combined using the Wilcoxon method in Seurat to identify cluster-specific marker genes. Each retained marker gene was expressed in a minimum of 25% of cells and at a minimum $\log_2$ fold change threshold of 0.25.

In paired cluster analyses, differentially expressed genes were considered significant if the adjusted p-value was less than 0.01 (Benjamini-Hochberg correction for multiple testing) and the absolute $\log_2$ expression fold change was ≥ 0.5.

Mapping cells between subpopulations in different samples

To compare subpopulations identified in the merged dataset (5 samples), we applied scGPS (single cell Global Projection between Subpopulations), a machine learning procedure to select optimal gene predictors and to build prediction models that can estimate between-subpopulation transition scores. The transition scores are the probability of cells from one subpopulation that are in the same class with the cells in the other subpopulation. The scores, therefore, estimate the similarity between any two subpopulations. Here, we compared three main subpopulations from sample Retina 2A with all subpopulations in the sample Retina 2B. The source code of the scGPS method is available with open-access (https://github.com/IMB-Computational-Genomics-Lab/scGPS).

Correlation of scRNA-seq data with retinal cell types

The mean expression levels of cells in each cluster were calculated and used to calculate Pearson's correlations in a pairwise manner with each of the other clusters and results were deemed significant if the correlation P-value was less than 0.01.

Pathway analysis

Enrichment analysis for significant differentially expressed genes detected per cluster was performed using Enrichr (Kuleshov *et al*, 2016). The combined score, computed by taking the log of p-value from the Fisher exact test and multiplying by the z-score of the deviation of the expected rank, was used to determine the enrichment ranking for pathways, ontologies, transcription factor network and protein network analysis.

Fluorescent in situ hybridization

Donor retinas were first dissected from the eye cup. The retinal tissues were subjected to 30% sucrose cryoprotection and were then frozen in -80°C. Sections were cut on a cryostat (Leica CM3050S) and mounted on glass slides (SuperFrostPlus). The retinal samples were fixed in 3.7% (vol/vol) formaldehyde and hybridized with Stellaris RNA FISH probes (Biosearch Technologies) against *MALAT1* labeled with Quasar 570, following the manufacturer's instructions. Briefly, samples were incubated with Quasar 570-labeled probes at 125nM in hybridization buffer and hybridized 5 hours at 37°C, followed by nuclear counterstain using DAPI. The samples are imaged using a ZEISS confocal laser-scanning microscope (ZEISS, LSM700).

Data availability

The raw and processed scRNA-seq files for this analysis are available at ArrayExpress under the accession number E-MTAB-7316 (http://www.ebi.ac.uk/arrayexpress/experiments/E-MTAB-7316).

Author Contributions

HW, AM coordinated and collected the human donor retinas, GP provided the funding for human donor tissue collection, LF, TN, JJ, SH, RW, LZ, TZ, UG conducted the experiments; SL, CL, AS, RW, QN, EW, JS, TL, LZ, TZ, UG processed and/or analysed the data; PYW, AH, JP, MG and RW contributed to experimental design and data analysis; SL, AH, JP and RW wrote the manuscript.

Acknowledgements

This publication is part of the Human Cell Atlas (www.humancellatlas.org/publications) and the ANZ Human Eye Cell Atlas Consortium. The human Müller cell line Moorfields/Institute of Ophthalmology- Müller 1 (MIO-M1) was obtained from the UCL Institute of Ophthalmology, London, UK. The authors want to thank David Mackey and Holly Chinnery for critical discussion and helpful feedback for this study, and Prema Finn for technical assistance for the collection of human donor samples. This work was supported by funding from the Ophthalmic Research Institute of Australia (RW, SL), the University of Melbourne De Brettville Trust (RW) and the Kel and Rosie Day Foundation (RW) and GOSHCC (JCS). The Centre for Eye Research Australia receives operational infrastructure support from the Victorian Government.

Competing Interests statement

The authors have no conflict of interest to declare.

References

Alvarez-Delfin K, Morris AC, Snelson CD, Gamse JT, Gupta T, Marlow FL, Mullins MC, Burgess HA, Granato M & Fadool JM (2009) Tbx2b is required for ultraviolet photoreceptor cell specification during zebrafish retinal development. *Proc. Natl. Acad. Sci. U. S. A.* **106:** 2023–2028

Baxter M, Withey S, Harrison S, Segeritz C-P, Zhang F, Atkinson-Dell R, Rowe C, Gerrard DT, Sison-Young R, Jenkins R, Henry J, Berry AA, Mohamet L, Best M, Fenwick SW, Malik H, Kitteringham NR, Goldring CE, Piper Hanley K, Vallier L, et al (2015) Phenotypic and functional analyses show stem cell-derived hepatocyte-like cells better mimic fetal rather than adult hepatocytes. *J. Hepatol.* **62:** 581–589

Blackshaw S, Fraioli RE, Furukawa T & Cepko CL (2001) Comprehensive analysis of photoreceptor gene expression and the identification of candidate retinal disease genes. *Cell*

107: 579–589

Boon CJF, den Hollander AI, Hoyng CB, Cremers FPM, Klevering BJ & Keunen JEE (2008) The spectrum of retinal dystrophies caused by mutations in the peripherin/RDS gene. *Prog. Retin. Eye Res.* **27:** 213–235

Butler A, Hoffman P, Smibert P, Papalexi E & Satija R (2018) Integrating single-cell transcriptomic data across different conditions, technologies, and species. *Nat. Biotechnol.* **36:** 411–420

Corbo JC, Myers CA, Lawrence KA, Jadhav AP & Cepko CL (2007) A typology of photoreceptor gene expression patterns in the mouse. *Proc. Natl. Acad. Sci. U. S. A.* **104:** 12069–12074

Dobin A, Davis CA, Schlesinger F, Drenkow J, Zaleski C, Jha S, Batut P, Chaisson M & Gingeras TR (2013) STAR: ultrafast universal RNA-seq aligner. *Bioinformatics* **29:** 15–21

Eldred KC, Hadyniak SE, Hussey KA, Brenerman B, Zhang P-W, Chamling X, Sluch VM, Welsbie DS, Hattar S, Taylor J, Wahlin K, Zack DJ & Johnston RJ Jr (2018) Thyroid hormone signaling specifies cone subtypes in human retinal organoids. *Science* **362:** Available at: http://dx.doi.org/10.1126/science.aau6348

Enright JM, Lawrence KA, Hadzic T & Corbo JC (2015) Transcriptome profiling of developing photoreceptor subtypes reveals candidate genes involved in avian photoreceptor diversification. *J. Comp. Neurol.* **523:** 649–668

Farkas MH, Grant GR, White JA, Sousa ME, Consugar MB & Pierce EA (2013a) Transcriptome analyses of the human retina identify unprecedented transcript diversity and 3.5 Mb of novel transcribed sequence via significant alternative splicing and novel genes. *BMC Genomics* **14:** 486

Farkas MH, Grant GR, White JA, Sousa ME, Consugar MB & Pierce EA (2013b) Transcriptome analyses of the human retina identify unprecedented transcript diversity and 3.5 Mb of novel transcribed sequence via significant alternative splicing and novel genes. *BMC Genomics* **14:** 486

Fernández-Sánchez L, Lax P, Campello L, Pinilla I & Cuenca N (2015) Astrocytes and Müller Cell Alterations During Retinal Degeneration in a Transgenic Rat Model of Retinitis

Pigmentosa. *Front. Cell. Neurosci.* **9:** 484

Gill KP, Hung SSC, Sharov A, Lo CY, Needham K, Lidgerwood GE, Jackson S, Crombie DE, Nayagam BA, Cook AL, Hewitt AW, Pébay A & Wong RCB (2016) Enriched retinal ganglion cells derived from human embryonic stem cells. *Sci. Rep.* **6:** 30552

Handel AE, Chintawar S, Lalic T, Whiteley E, Vowles J, Giustacchini A, Argoud K, Sopp P, Nakanishi M, Bowden R, Cowley S, Newey S, Akerman C, Ponting CP & Cader MZ (2016) Assessing similarity to primary tissue and cortical layer identity in induced pluripotent stem cell-derived cortical neurons through single-cell transcriptomics. *Hum. Mol. Genet.* **25:** 989–1000

Hollborn M, Ulbricht E, Rillich K, Dukic-Stefanovic S, Wurm A, Wagner L, Reichenbach A, Wiedemann P, Limb GA, Bringmann A & Kohen L (2011) The human Müller cell line MIO-M1 expresses opsins. *Mol. Vis.* **17:** 2738–2750

Hornan DM, Peirson SN, Hardcastle AJ, Molday RS, Cheetham ME & Webster AR (2007a) Novel retinal and cone photoreceptor transcripts revealed by human macular expression profiling. *Invest. Ophthalmol. Vis. Sci.* **48:** 5388–5396

Hornan DM, Peirson SN, Hardcastle AJ, Molday RS, Cheetham ME & Webster AR (2007b) Novel retinal and cone photoreceptor transcripts revealed by human macular expression profiling. *Invest. Ophthalmol. Vis. Sci.* **48:** 5388–5396

Hoshino A, Ratnapriya R, Brooks MJ, Chaitankar V, Wilken MS, Zhang C, Starostik MR, Gieser L, La Torre A, Nishio M, Bates O, Walton A, Bermingham-McDonogh O, Glass IA, Wong ROL, Swaroop A & Reh TA (2017) Molecular Anatomy of the Developing Human Retina. *Dev. Cell* **43:** 763–779.e4

Hung SSC, Khan S, Lo CY, Hewitt AW & Wong RCB (2017) Drug discovery using induced pluripotent stem cell models of neurodegenerative and ocular diseases. *Pharmacol. Ther.* **177:** 32–43

Ilicic T, Kim JK, Kolodziejczyk AA, Bagger FO, McCarthy DJ, Marioni JC & Teichmann SA (2016) Classification of low quality cells from single-cell RNA-seq data. *Genome Biol.* **17:** 29

Imanishi Y, Li N, Sokal I, Sowa ME, Lichtarge O, Wensel TG, Saperstein DA, Baehr W &

Palczewski K (2002) Characterization of retinal guanylate cyclase-activating protein 3 (GCAP3) from zebrafish to man. *Eur. J. Neurosci.* **15:** 63–78

Jeon CJ, Strettoi E & Masland RH (1998) The major cell populations of the mouse retina. *J. Neurosci.* **18:** 8936–8946

Klimova L, Antosova B, Kuzelova A, Strnad H & Kozmik Z (2015) Onecut1 and Onecut2 transcription factors operate downstream of Pax6 to regulate horizontal cell development. *Dev. Biol.* **402:** 48–60

Kobayashi W, Onishi A, Tu H-Y, Takihara Y, Matsumura M, Tsujimoto K, Inatani M, Nakazawa T & Takahashi M (2018) Culture Systems of Dissociated Mouse and Human Pluripotent Stem Cell-Derived Retinal Ganglion Cells Purified by Two-Step Immunopanning. *Invest. Ophthalmol. Vis. Sci.* **59:** 776–787

Kowalczyk MS, Tirosh I, Heckl D, Rao TN, Dixit A, Haas BJ, Schneider RK, Wagers AJ, Ebert BL & Regev A (2015) Single-cell RNA-seq reveals changes in cell cycle and differentiation programs upon aging of hematopoietic stem cells. *Genome Res.* **25:** 1860–1872

Kozulin P, Natoli R, O'Brien KMB, Madigan MC & Provis JM (2009) Differential expression of anti-angiogenic factors and guidance genes in the developing macula. *Mol. Vis.* **15:** 45–59

Kuleshov MV, Jones MR, Rouillard AD, Fernandez NF, Duan Q, Wang Z, Koplev S, Jenkins SL, Jagodnik KM, Lachmann A, McDermott MG, Monteiro CD, Gundersen GW & Ma'ayan A (2016) Enrichr: a comprehensive gene set enrichment analysis web server 2016 update. *Nucleic Acids Res.* **44:** W90–7

Lakowski J, Welby E, Budinger D, Di Marco F, Di Foggia V, Bainbridge JWB, Wallace K, Gamm DM, Ali RR & Sowden JC (2018) Isolation of Human Photoreceptor Precursors via a Cell Surface Marker Panel from Stem Cell-Derived Retinal Organoids and Fetal Retinae. *Stem Cells* Available at: http://dx.doi.org/10.1002/stem.2775

Lawrence JM, Singhal S, Bhatia B, Keegan DJ, Reh TA, Luthert PJ, Khaw PT & Limb GA (2007) MIO-M1 cells and similar muller glial cell lines derived from adult human retina exhibit neural stem cell characteristics. *Stem Cells* **25:** 2033–2043

Liao J-L, Yu J, Huang K, Hu J, Diemer T, Ma Z, Dvash T, Yang X-J, Travis GH, Williams DS, Bok D & Fan G (2010) Molecular signature of primary retinal pigment epithelium and stem-cell-derived RPE cells. *Hum. Mol. Genet.* **19:** 4229–4238

Li H-B, You Q-S, Xu L-X, Sun L-X, Abdul Majid AS, Xia X-B & Ji D (2017) Long Non-Coding RNA-MALAT1 Mediates Retinal Ganglion Cell Apoptosis Through the PI3K/Akt Signaling Pathway in Rats with Glaucoma. *Cell. Physiol. Biochem.* **43:** 2117–2132

Limb GA, Salt TE, Munro PMG, Moss SE & Khaw PT (2002) In vitro characterization of a spontaneously immortalized human Müller cell line (MIO-M1). *Invest. Ophthalmol. Vis. Sci.* **43:** 864–869

Lun ATL, Bach K & Marioni JC (2016) Pooling across cells to normalize single-cell RNA sequencing data with many zero counts. *Genome Biol.* **17:** 75

Macosko EZ, Basu A, Satija R, Nemesh J, Shekhar K, Goldman M, Tirosh I, Bialas AR, Kamitaki N, Martersteck EM, Trombetta JJ, Weitz DA, Sanes JR, Shalek AK, Regev A & McCarroll SA (2015) Highly Parallel Genome-wide Expression Profiling of Individual Cells Using Nanoliter Droplets. *Cell* **161:** 1202–1214

Masuda T, Sankowski R, Staszewski O, Böttcher C, Amann L, Scheiwe C, Nessler S, Kunz P, van Loo G, Coenen VA, Reinacher PC, Michel A, Sure U, Gold R, Priller J, Stadelmann C & Prinz M (2019) Spatial and temporal heterogeneity of mouse and human microglia at single-cell resolution. *Nature* **566:** 388–392

Mustafi D, Kevany BM, Bai X, Golczak M, Adams MD, Wynshaw-Boris A & Palczewski K (2016a) Transcriptome analysis reveals rod/cone photoreceptor specific signatures across mammalian retinas. *Hum. Mol. Genet.* **25:** 4376–4388

Mustafi D, Kevany BM, Bai X, Golczak M, Adams MD, Wynshaw-Boris A & Palczewski K (2016b) Transcriptome analysis reveals rod/cone photoreceptor specific signatures across mammalian retinas. *Hum. Mol. Genet.* **25:** 4376–4388

Ng L, Hurley JB, Dierks B, Srinivas M, Saltó C, Vennström B, Reh TA & Forrest D (2001) A thyroid hormone receptor that is required for the development of green cone photoreceptors. *Nat. Genet.* **27:** 94–98

Peng Y-R, Shekhar K, Yan W, Herrmann D, Sappington A, Bryman GS, van Zyl T, Do MTH, Regev A & Sanes JR (2019) Molecular Classification and Comparative Taxonomics of Foveal and Peripheral Cells in Primate Retina. *Cell* **176:** 1222–1237.e22

Phillips MJ, Jiang P, Howden S, Barney P, Min J, York NW, Chu L-F, Capowski EE, Cash A, Jain S, Barlow K, Tabassum T, Stewart R, Pattnaik BR, Thomson JA & Gamm DM (2018) A Novel Approach to Single Cell RNA-Sequence Analysis Facilitates In Silico Gene Reporting of Human Pluripotent Stem Cell-Derived Retinal Cell Types. *Stem Cells* **36:** 313–324

Pinelli M, Carissimo A, Cutillo L, Lai C-H, Mutarelli M, Moretti MN, Singh MV, Karali M, Carrella D, Pizzo M, Russo F, Ferrari S, Ponzin D, Angelini C, Banfi S & di Bernardo D (2016a) An atlas of gene expression and gene co-regulation in the human retina. *Nucleic Acids Res.* **44:** 5773–5784

Pinelli M, Carissimo A, Cutillo L, Lai C-H, Mutarelli M, Moretti MN, Singh MV, Karali M, Carrella D, Pizzo M, Russo F, Ferrari S, Ponzin D, Angelini C, Banfi S & di Bernardo D (2016b) An atlas of gene expression and gene co-regulation in the human retina. *Nucleic Acids Res.* **44:** 5773–5784

Robinson MD & Oshlack A (2010) A scaling normalization method for differential expression analysis of RNA-seq data. *Genome Biol.* **11:** R25

Roorda A & Williams DR (1999) The arrangement of the three cone classes in the living human eye. *Nature* **397:** 520–522

Shekhar K, Lapan SW, Whitney IE, Tran NM, Macosko EZ, Kowalczyk M, Adiconis X, Levin JZ, Nemesh J, Goldman M, McCarroll SA, Cepko CL, Regev A & Sanes JR (2016) Comprehensive Classification of Retinal Bipolar Neurons by Single-Cell Transcriptomics. *Cell* **166:** 1308–1323.e30

Sluch VM, Davis C-HO, Ranganathan V, Kerr JM, Krick K, Martin R, Berlinicke CA, Marsh-Armstrong N, Diamond JS, Mao H-Q & Zack DJ (2015) Differentiation of human ESCs to retinal ganglion cells using a CRISPR engineered reporter cell line. *Sci. Rep.* **5:** 16595

Soto I, Oglesby E, Buckingham BP, Son JL, Roberson EDO, Steele MR, Inman DM, Vetter ML, Horner PJ & Marsh-Armstrong N (2008) Retinal Ganglion Cells Downregulate Gene Expression and Lose Their Axons within the Optic Nerve Head in a Mouse Glaucoma Model. *Journal of Neuroscience* **28:** 548–561

Stoeckius M, Hafemeister C, Stephenson W, Houck-Loomis B, Chattopadhyay PK, Swerdlow H, Satija R & Smibert P (2017) Simultaneous epitope and transcriptome measurement in single cells. *Nat. Methods* **14:** 865

Strunnikova NV, Maminishkis A, Barb JJ, Wang F, Zhi C, Sergeev Y, Chen W, Edwards AO, Stambolian D, Abecasis G, Swaroop A, Munson PJ & Miller SS (2010) Transcriptome analysis and molecular signature of human retinal pigment epithelium. *Hum. Mol. Genet.* **19:** 2468–2486

Subirada PV, Paz MC, Ridano ME, Lorenc VE, Vaglienti MV, Barcelona PF, Luna JD & Sánchez MC (2018) A journey into the retina: Müller glia commanding survival and death. *Eur. J. Neurosci.* **47:** 1429–1443

Vecino E, Rodriguez FD, Ruzafa N, Pereiro X & Sharma SC (2016) Glia-neuron interactions in the mammalian retina. *Prog. Retin. Eye Res.* **51:** 1–40

Viets K, Eldred K & Johnston RJ Jr (2016) Mechanisms of Photoreceptor Patterning in Vertebrates and Invertebrates. *Trends Genet.* **32:** 638–659

Voigt AP, Whitmore SS, Flamme-Wiese MJ, Riker MJ, Wiley LA, Tucker BA, Stone EM, Mullins RF & Scheetz TE (2019) Molecular characterization of foveal versus peripheral human retina by single-cell RNA sequencing. *Exp. Eye Res.* **184:** 234–242

Wan P, Su W & Zhuo Y (2017) Precise long non-coding RNA modulation in visual maintenance and impairment. *J. Med. Genet.* **54:** 450–459

Welby E, Lakowski J, Di Foggia V, Budinger D, Gonzalez-Cordero A, Lun ATL, Epstein M, Patel A, Cuevas E, Kruczek K, Naeem A, Minneci F, Hubank M, Jones DT, Marioni JC, Ali RR & Sowden JC (2017) Isolation and Comparative Transcriptome Analysis of Human Fetal and iPSC-Derived Cone Photoreceptor Cells. *Stem Cell Reports* **9:** 1898–1915

Whitmore SS, Wagner AH, DeLuca AP, Drack AV, Stone EM, Tucker BA, Zeng S, Braun TA, Mullins RF & Scheetz TE (2014a) Transcriptomic analysis across nasal, temporal, and macular regions of human neural retina and RPE/choroid by RNA-Seq. *Exp. Eye Res.* **129:** 93–106

Whitmore SS, Wagner AH, DeLuca AP, Drack AV, Stone EM, Tucker BA, Zeng S, Braun TA, Mullins RF & Scheetz TE (2014b) Transcriptomic analysis across nasal, temporal, and macular regions of human neural retina and RPE/choroid by RNA-Seq. *Exp. Eye Res.* **129:**

93–106

Wirsching H-G, Krishnan S, Florea A-M, Frei K, Krayenbühl N, Hasenbach K, Reifenberger G, Weller M & Tabatabai G (2013) Thymosin beta 4 gene silencing decreases stemness and invasiveness in glioblastoma. *Brain* **137:** 433–448

Yang S, Yao H, Li M, Li H & Wang F (2016) Long Non-Coding RNA MALAT1 Mediates Transforming Growth Factor Beta1-Induced Epithelial-Mesenchymal Transition of Retinal Pigment Epithelial Cells. *PLoS One* **11:** e0152687

Yoshida S, Mears AJ, Friedman JS, Carter T, He S, Oh E, Jing Y, Farjo R, Fleury G, Barlow C, Hero AO & Swaroop A (2004) Expression profiling of the developing and mature Nrl −/− mouse retina: identification of retinal disease candidates and transcriptional regulatory targets of Nrl. *Hum. Mol. Genet.* **13:** 1487–1503

Zheng GXY, Terry JM, Belgrader P, Ryvkin P, Bent ZW, Wilson R, Ziraldo SB, Wheeler TD, McDermott GP, Zhu J, Gregory MT, Shuga J, Montesclaros L, Underwood JG, Masquelier DA, Nishimura SY, Schnall-Levin M, Wyatt PW, Hindson CM, Bharadwaj R, et al (2017) Massively parallel digital transcriptional profiling of single cells. *Nat. Commun.* **8:** 14049

Figure Legends

Figure 1: Single cell transcriptome atlas for human neural retina.

(A, B) t-SNE visualization of 20,009 human retinal cells colored by (A) annotation of 18 transcriptionally distinct clusters (C0-C17) and (B) their distribution in 3 donor retina samples.

C) Feature expression heatmap showing expression patterns of major retinal class markers across 16 retinal cell clusters. The size of each circle depicts the percentage of cells expressing the marker within the cluster. Brown colour indicates ≥10 nTrans (number of transcripts).

D) t-SNE plots showing expression of a set of selected marker genes for major retinal classes.

E) Correlation matrix for the identified 18 clusters. The upper triangle depicts the z-value for correlation and the lower triangle depicts the correlation coefficient for gene expression in clusters.

F) Heatmap of differentially expressed genes used to classify cell types for each cluster compared to all other clusters for the 18 retinal cell clusters. The rows correspond to top 10 genes most selectively upregulated in individual clusters ($p< 0.01$, Benjamini-Hochberg correction) and the columns show individual cells ordered by cluster (C0-C17).

Figure 2: Identification of *MALAT1-hi* and *MALAT1-lo* subpopulations of rod photoreceptors.

A) Feature expression heatmap of a panel of known marker genes for rod photoreceptors across the identified 16 retinal cell clusters. Brown colour indicates ≥100 nTrans (number of transcripts).

B) Representation of the three donor retina samples in the six rod photoreceptor clusters.

C) Violin plot showing high or low expression levels of *MALAT1* in rod photoreceptor clusters.

D) Distribution of rod photoreceptor populations with high MALAT1 expression (*MALAT1*-hi) or low *MALAT1* expression (*MALAT1*-lo) in three donor retina samples.

E) Fluorescent in situ hybridization analysis of human peripheral retina showing heterogeneous levels of *MALAT1* expression in the rod photoreceptors located in the outer nuclear layer (ONL). INL: inner nuclear layer; OPL: outer plexiform layer. Scale bar = 20μm.

Figure 3: *MALAT1* subpopulations of rod photoreceptors is not due to donor variation. Canonical correlation analysis was used to effectively correct donor-specific variations in rod photoreceptors.

A, B) (A) t-SNE visualization of human retinal cells colored by annotation of 13 transcriptionally distinct clusters (CCA0-CCA12) and (B) their distribution in 3 donor retina samples.

C) Feature expression heatmap showing expression patterns of 7 rod photoreceptor markers across 12 retinal cell clusters. The size of each circle depicts the percentage of cells expressing the marker within the cluster. Brown colour indicates ≥50 nTrans (number of transcripts).

D) t-SNE plots showing expression of *MALAT1*.

E) Expression pattern of *MALAT1* in the rod photoreceptor showing *MALAT1-hi* (CCA1, CCA10) and *MALAT1-lo* (CCA0) subpopulations. x-axis depicts normalized transcript levels.

F) t-SNE plots showing expression of major ribosomal genes.

G) Heatmap of differentially expressed genes between the two *MALAT1-hi* clusters CCA1 and CCA10. The rows correspond to top 10 genes most selectively upregulated in individual clusters (p< 0.01, Benjamini-Hochberg correction) and the columns show individual cells ordered in CCA1 and CCA10.

Figure 4: Loss of *MALAT1* expression in rod photoreceptors with longer post-mortem time. Fluorescent in situ hybridization analysis of the same donor human peripheral retina at different time points post-mortem (7 and 13 hours, Retina 7), showing decreases in *MALAT1-hi* rod subpopulations in the outer nuclear layer (ONL) at later time point. INL: inner nuclear layer; OPL: outer plexiform layer. Scale bar = 20µm. White arrows indicated *MALAT1-hi* rod photoreceptors.

Figure 5: Assessment of cone photoreceptor and glial cell types in human retina .

A) Feature expression heatmap showing the expression of 11 known cone photoreceptor markers across 16 retinal cell clusters. Brown colour indicates ≥10 nTrans (number of transcripts).

B) The proportion of cone photoreceptor subtypes identified in population C10, based on expression of *OPN1LW / OPN1MW* (L/M cones) and *OPN1SW* (S cones).

C) Scatter plots showing expression of *OPN1LW/OPN1MW* or *OPN1SW* in individual cone photoreceptors for population C10. The colour depicts expression level for *OPN1LW/OPN1MW* in individual cells.

D) Heatmap of top 20 differentially expressed genes between L/M cones and S cones. The colour depicts normalised gene expression (z-score capped at 2.5).

E) Expression pattern of glial markers in Muller glia (C9) and retinal astrocytes (C16). x-axis depicts normalized transcript levels.

Figure 6: Benchmarking retinal cells using the human neural retina atlas.

A) Correlation analysis of scRNA-seq data of hiPSC-derived cone photoreceptors (week 15) against fetal cone photoreceptors (Welby *et al*, 2017), as well as adult cone and rod photoreceptors from this human neural retina atlas.

B) Principal component analysis to assess transcriptome similarity of hiPSC-derived cone photoreceptors to fetal and adult photoreceptors.

C) t-SNE analysis of the human Müller glia cell line MIO-M1 with the retinal cell types identified in this human neural retina atlas.

D) Correlation analysis of MIO-M1 with all major human retinal cell types.

E) Top ranked differentially expressed genes identified in MIO-M1 compared to other retinal cell types based on logistic regression score.

Expanded View Figure Legends:

Figure EV1: Bipolar marker gene expression in the compiled human neural retina transcriptome atlas (20,009 cells).

A) Feature expression heatmap of VSX2 (pan-bipolar), ISL1 (ON-bipolar), GRIK1 (OFF-bipolar), PRKCA (rod bipolar cells) and TTR (DB4 bipolar).

B) t-SNE plots showing gene expression for 14 new markers for individual bipolar subtypes identified in previous mouse scRNA-seq study (Shekhar *et al*, 2016).

Figure EV2: Amacrine marker gene expression in the compiled human neural retina transcriptome atlas (20,009 cells).

A, B) t-SNE plots showing gene expression in the compiled human retina transcriptome atlas (20,009 cells). (A) 10 commonly used amacrine markers and (B) new markers for amacrine subtypes identified in previous mouse scRNA-seq study (Macosko *et al*, 2015).

Figure EV3: MALAT1 expression in human retina.

A) Fluorescent in situ hybridization showing expression of *MALAT1* in three donor retina samples (Retina 4-6). Retina 5 from Figure 2E is also displayed here for easier comparison. Green arrows highlight rod photoreceptors with low levels of *MALAT1* in Retina 4 and 6, white arrows highlight rod photoreceptors with high levels of *MALAT1* in Retina 5. Scale bars = 20µm.

B) Correlation of proportion of MALAT1-hi rod populations with time of retina retrieval after death for Retina 1-3.

Figure EV4: Cell cycle scores for major retinal cell types.

Commented [KV1]: Please provide figure title

Cell cycle scores across major retinal cell clusters showing the likelihood for the proportion of cells in G1, S or G2/M phases.

Figure EV 5: Using the human neural retinal transcriptome atlas as a benchmark.

Correlation matrix to benchmark hiPSC-derived cone photoreceptors (week 15, week 20; (Welby *et al*, 2017), fetal cone photoreceptors (Welby *et al*, 2017), adult retina (Phillips *et al*, 2018) and the human Müller glia cell line MIO-M1 against all retinal cell types identified in this human neural retina atlas.

Figure EV1

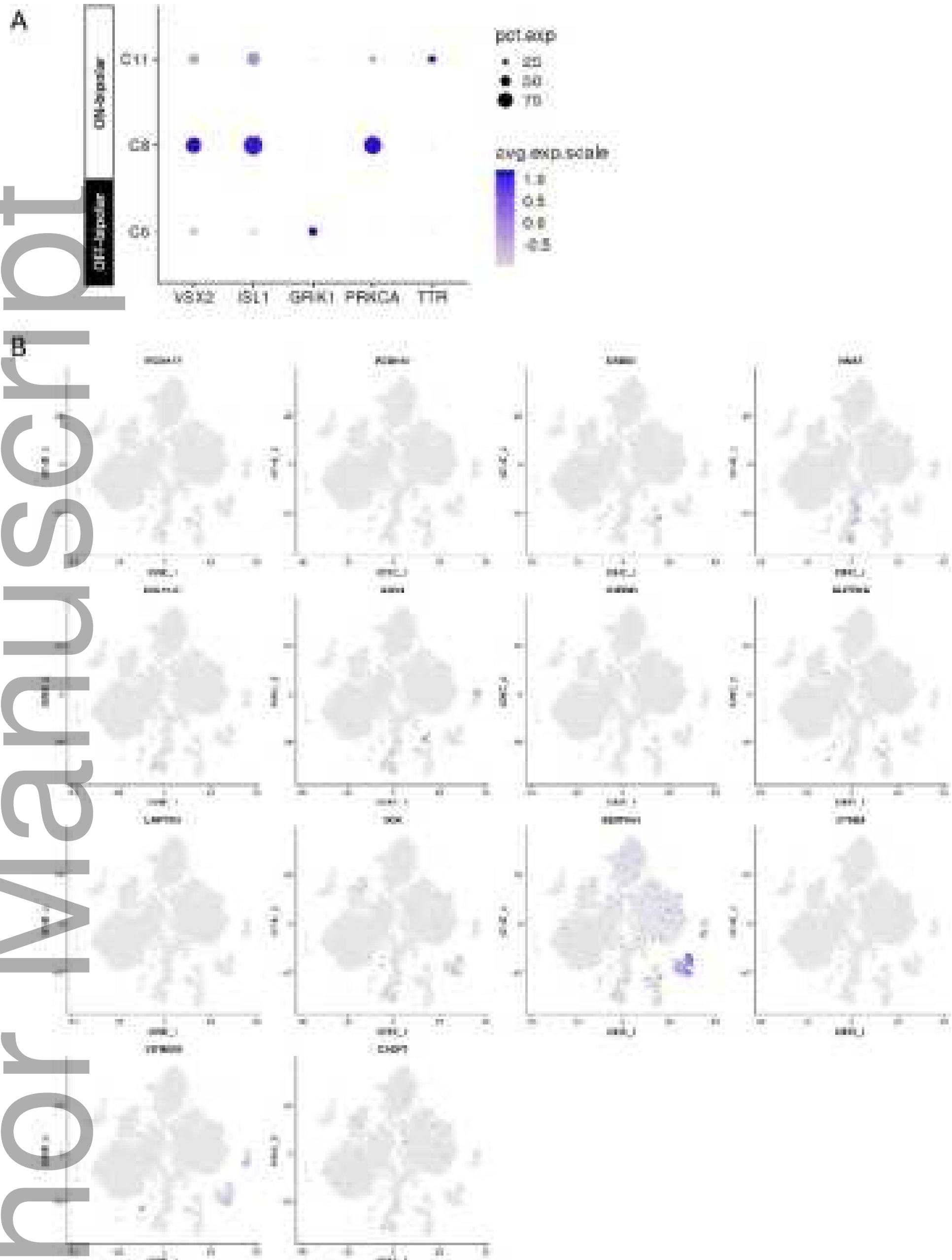

embj_2018100811_f1ev.jpg

Figure EV2

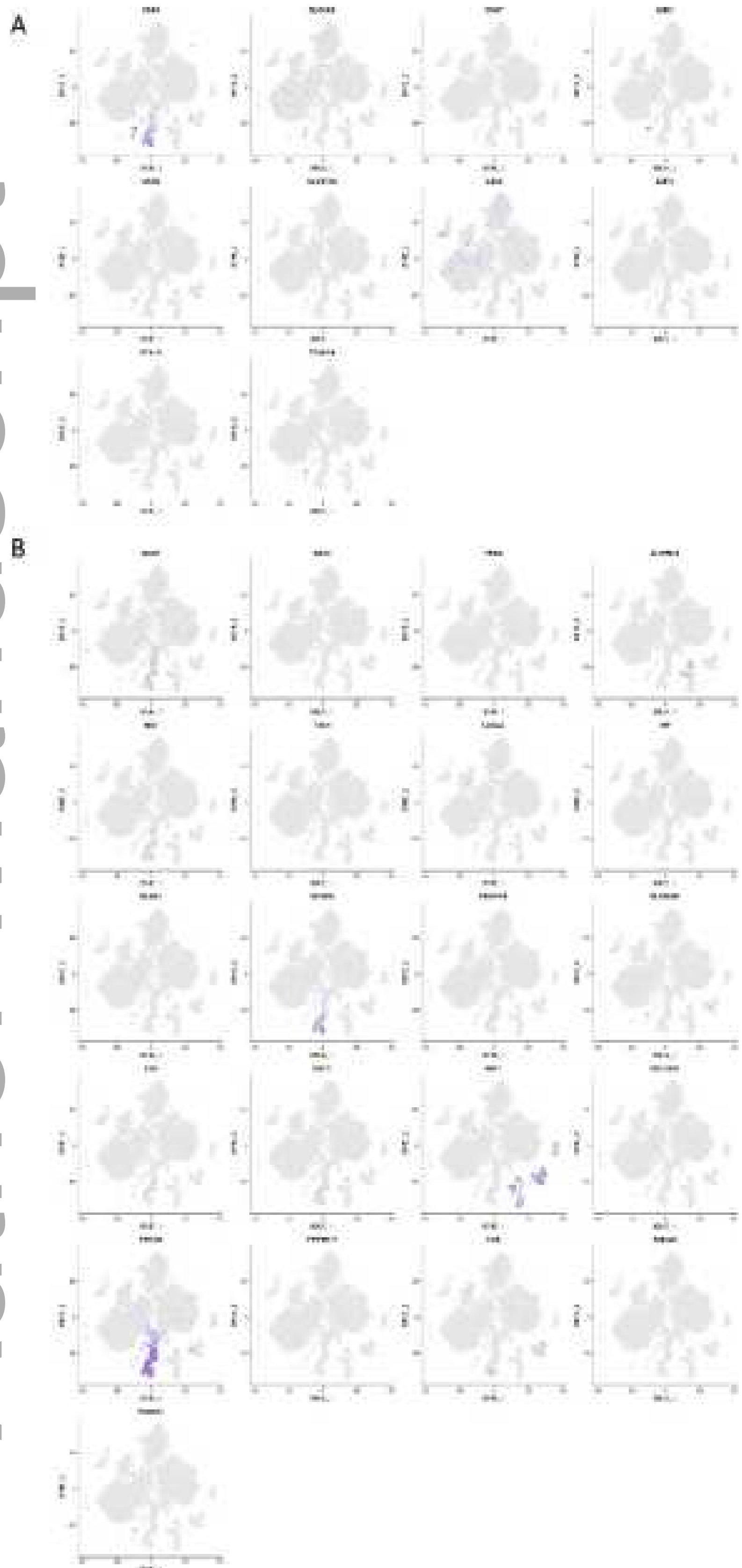

embj_2018100811_f2ev.jpg

Figure EV3

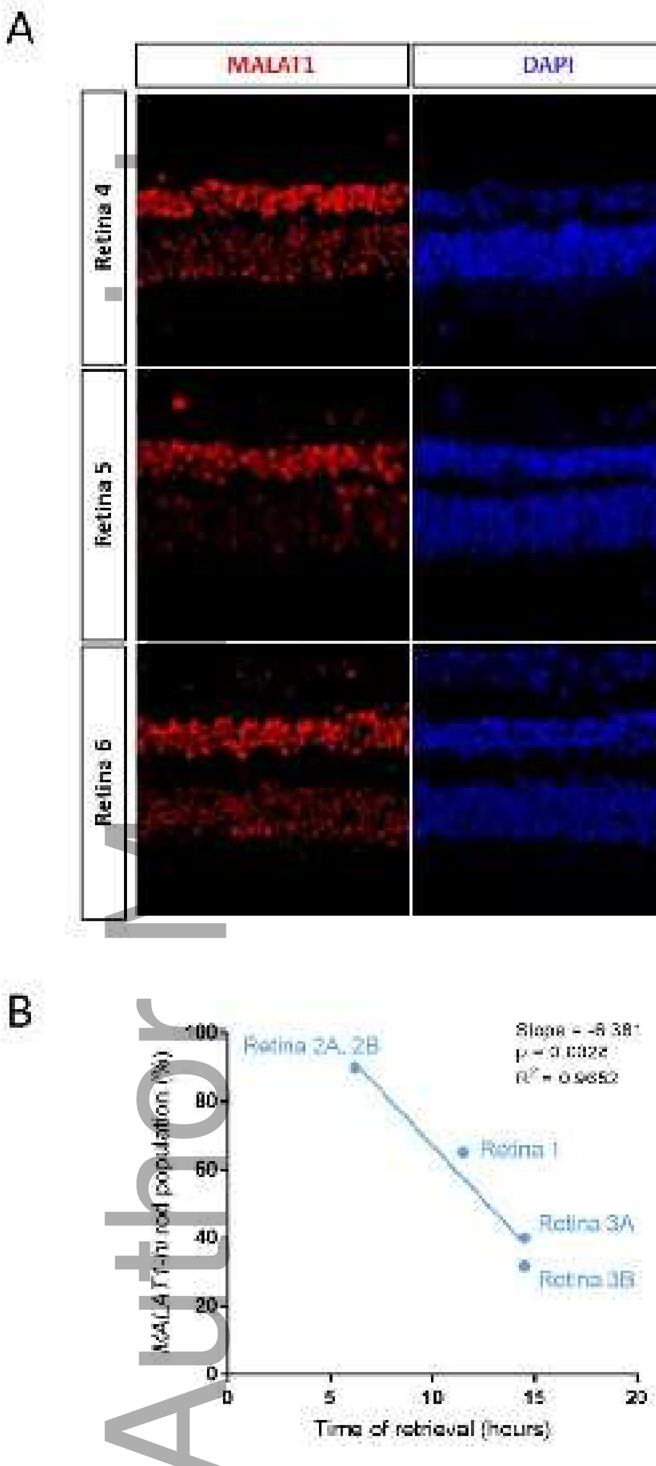

embj_2018100811_f3ev.jpg

Figure EV4

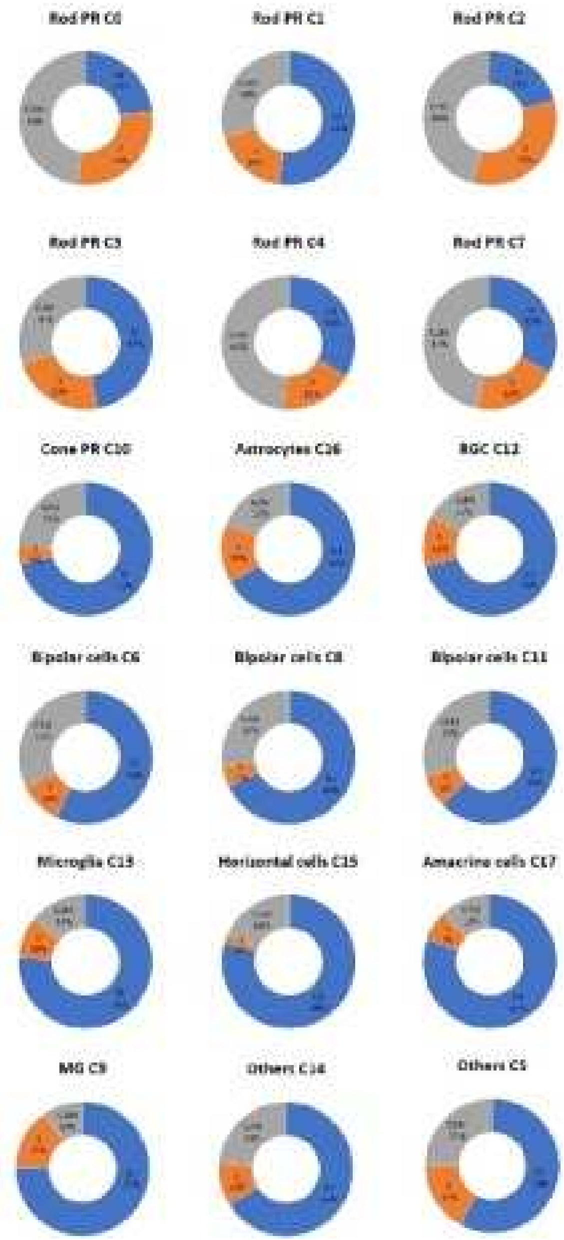

embj_2018100811_f4ev.jpg

Figure EV5

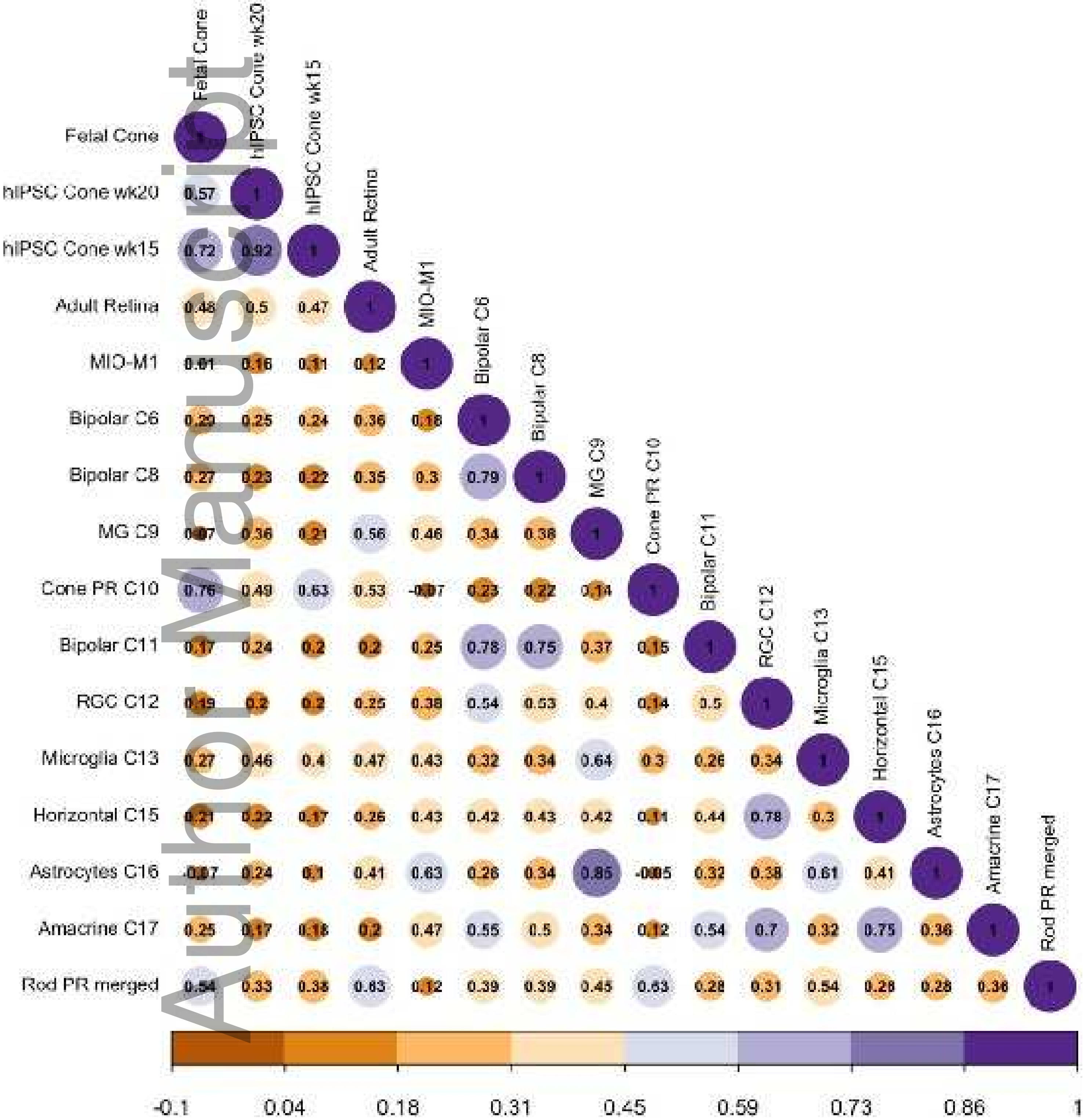

embj_2018100811_f5ev.jpg

Figure 1

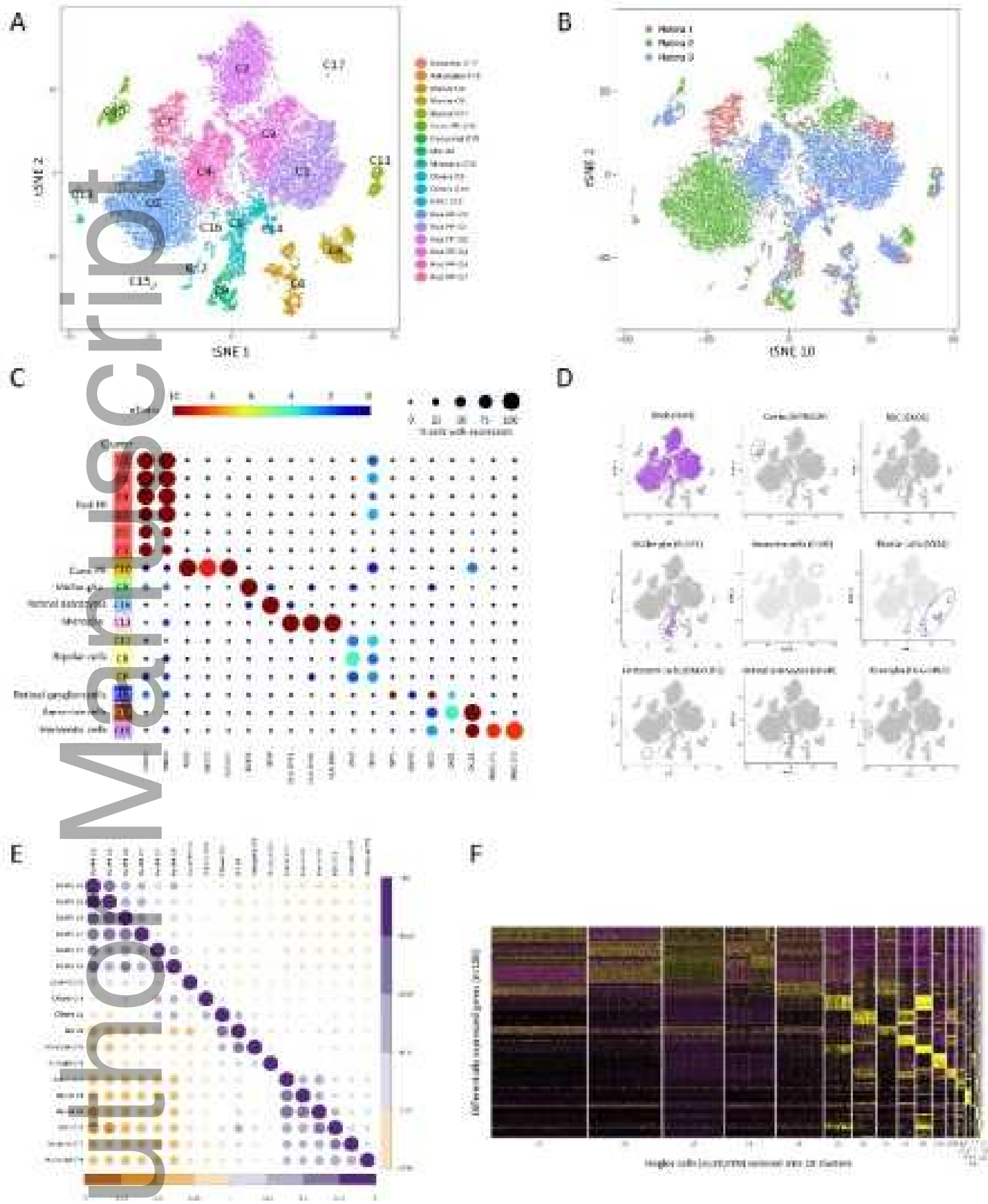

embj_2018100811_f1.jpg

Figure 2

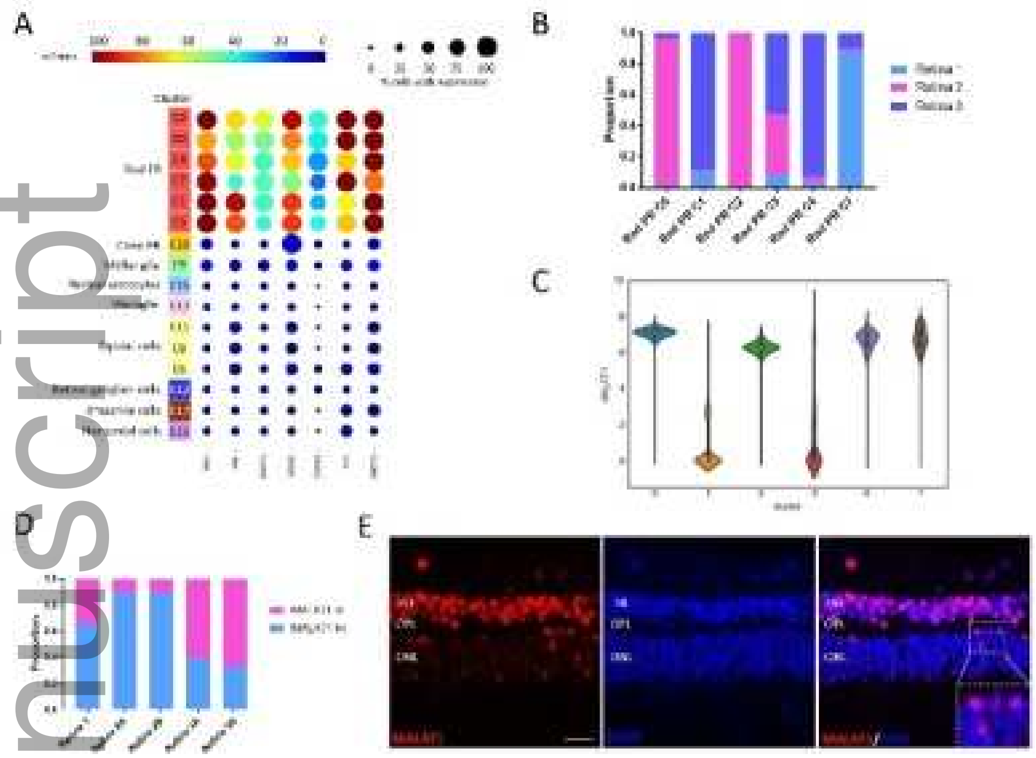

embj_2018100811_f2.jpg

Figure 3

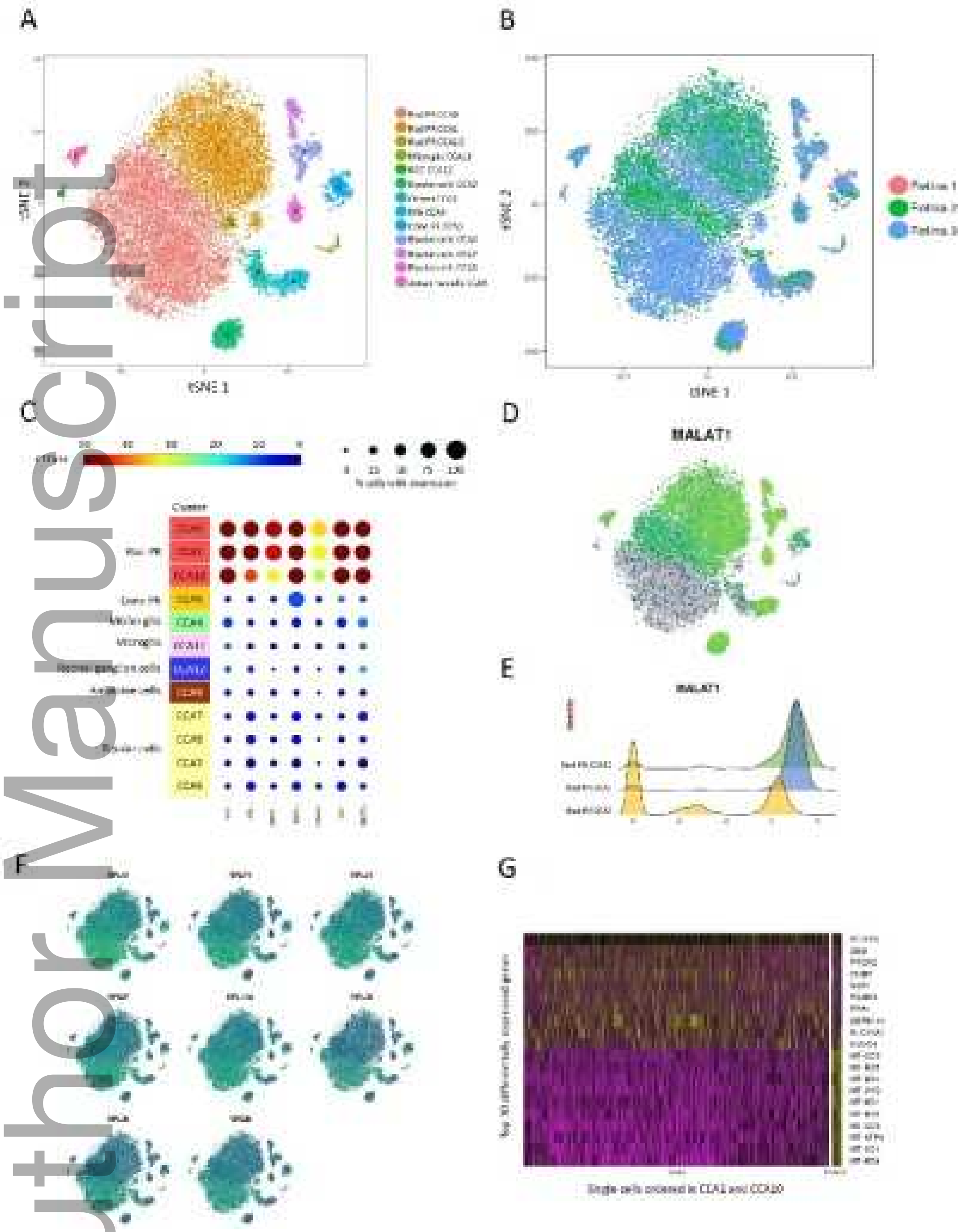

embj_2018100811_f3.jpg

Figure 4

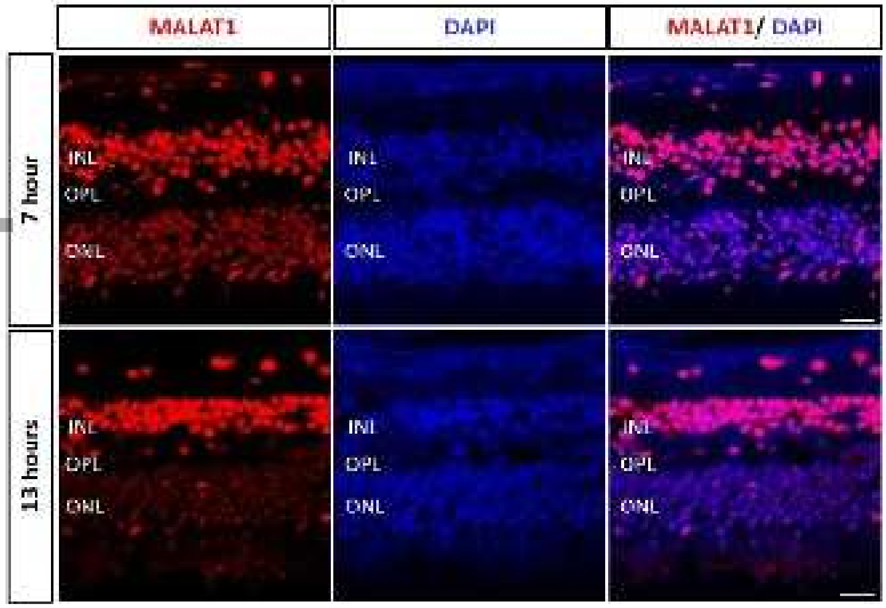

embj_2018100811_f4.jpg

Figure 5

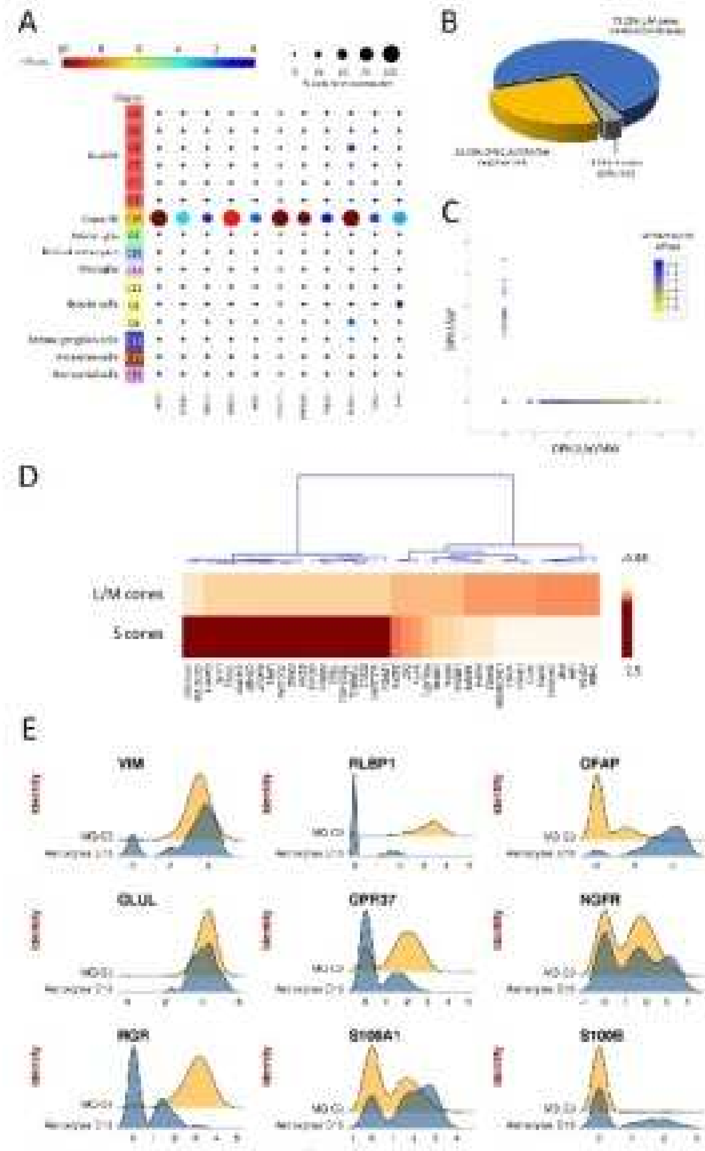

embj_2018100811_f5.jpg

Figure 6

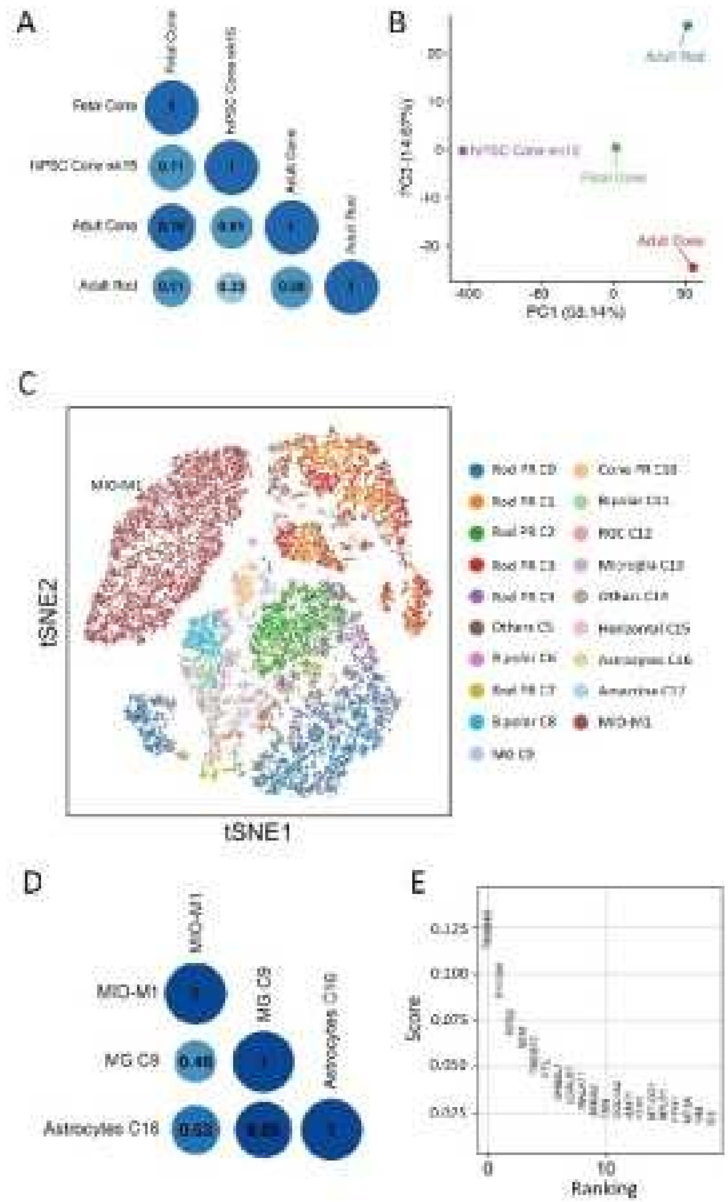

embj_2018100811_f6.jpg